Structural organization of cardiolipin-containing vesicles as models of the bacterial cytoplasmic membrane

Alessandra Luchini [a,†*], *Domenico Cavasso* [b], *Aurel Radulescu* [c], *Gerardino D'Errico* [b,d], *Luigi Paduano* [b,d], *Giuseppe Vitiello* [e,d*]

[a] Niels Bohr Institute, University of Copenhagen, Universitetsparken 5, 2100 Copenhagen, Denmark.

[b] Department of Chemical Science, University of Naples Federico II, Complesso di Monte Sant'Angelo, via Cinthia 4, 80126 Naples, Italy.

[c] Jülich Centre for Neutron Science, Garching Forschungszentrum, Lichtenbergstrasse 1, D-85747 Garching bei München, Germany.

[d] CSGI, Center for Colloid and Surface Science, via della Lastruccia 3, 50019 Sesto Fiorentino (FI), Italy.

[e] Department of Chemical, Materials and Production Engineering, University of Naples Federico II, Piazzale Tecchio 80, 80125 Naples, Italy.

ABSTRACT. The bacterial cytoplasmic membrane is the most inner bacterial membrane and is mainly composed of three different phospholipid species, i.e. phosphoethanolamine (PE), phosphoglycerol (PG) and cardiolipin (CL). In particular, PG and CL are responsible for the negative charge of the membrane and are often the targets of cationic antimicrobial agents. The growing resistance of bacteria towards the available antibiotics requires the development of new and more efficient antibacterial drugs. In this context, studying the physico-chemical properties of the bacterial cytoplasmic membrane is pivotal for understanding drug-membrane interactions at the molecular level as well as for designing drug-testing platforms. Here, we discuss the preparation and characterization of PE/PG/CL vesicle suspensions, which contain all the main

lipid components of the bacterial cytoplasmic membrane. The vesicle suspensions were characterized by means of small angle neutron scattering, dynamic light scattering and electron paramagnetic spectroscopy. By combining solution scattering and spectroscopy techniques, we proposed a detailed description of the impact of different CL concentrations on the structure and dynamics of the PE/PG bilayer. CL induces the formation of thicker bilayers, which exhibit ~~a~~ higher curvature and are overall more fluid. The experimental results contribute to shed light on the structure and dynamics of relevant model systems of the bacterial cytoplasmic membrane.

Keywords: cardiolipin, lipids, biomembranes, dynamic light scattering, small-angle neutron scattering, electron paramagnetic resonance.

Introduction

The bacterial cytoplasmic membrane is the most inner bacterial membrane and is mainly composed of lipids and proteins that are responsible for vital biological functions. Because of its fundamental role in the bacteria life, the cytoplasmic membrane is often the target of several antimicrobial agents, which are mainly designed to interact with its lipid components. [1] The bacterial cytoplasmic membrane has a simpler lipid composition than eukaryotic cell membranes [2], although it still includes several different lipid species. In particular, phospholipids are the most abundant and can be divided into three principal categories according to their headgroup chemical composition: phosphoethanolamine (PE), phosphoglycerol (PG) and diphosphoglycerol (DPG) lipids. [3] Different acyl chains are bound to the above listed headgroups and typically exhibit 12-20 C atoms and have 0-2 unsaturations. [4] Among the phospholipid acyl chains, cyclopropane fatty acids are also present, and they are more common in Gram-negative bacteria [5].

PE and PG headgroups are typically bound to two acyl chains and form di-tailed phospholipids. On the other hand, the DPG headgroup is normally associated with four acyl chains, forming the phospholipid known as cardiolipin (CL). Although, CL is a minor component in both eukaryotic and prokaryotic membranes, its important biological function is believed to include segregation of membrane domains, cross-linking of protein subdomains and formation of non-lamellar structures.[6] The amount of the different phospholipid species in the bacterial cytoplasmic membrane is highly variable from one bacterial type to another and it is also subject to change depending on environmental conditions such as pH, osmotic pressure, and temperature. In general, the PE content varies from 30-70 mol % of the total lipids in the cytoplasmic membrane, while PG and CL content is in the range of 20-60 mol % and 5-25 mol %, respectively. [7]

Because of the increasing resistance towards conventional antibiotics, the development of new and more efficient antimicrobial agents is a growing research field. Most of the proposed antimicrobial agents target bacterial membranes and induce their lysis [8]. However, understanding drug-membrane interaction at the molecular level requires a detailed characterization of the physico-chemical properties of bacterial membranes.

In general, direct investigation of biological membranes with biophysical and physico-chemical methods is often limited by the compositional complexity of the native membranes, which prevents the production of samples fulfilling the requirements of the characterization method of choice, e.g. low polydispersity or incorporation of a probe. From this perspective, model membrane systems, such as vesicles, offer several advantages including controlled and tunable composition and size distribution, which enable the correlation between the concentration of a specific membrane component and the observed membrane properties. Here, we discuss the structural and dynamic characterization of small unilamellar vesicles as model systems of bacterial cytoplasmic

membranes. The investigated vesicles were prepared with tertiary mixtures of 1-palmitoyl-2-oleoyl-sn-glycero-3- phosphoethanolamine (POPE), 1-palmitoyl-2-oleoyl-sn-glycero-3-phospho-(1'-rac-glycerol) (POPG) and CL (Figure 1), which include the three main lipid classes composing the bacterial cytoplasmic membrane, and therefore are a biologically relevant model system.

Most of the physico-chemical and biophysical studies on lipid bilayers mimicking the bacterial cytoplasmic membrane focused on the behavior of only 1-2 lipid components. The phase diagram of pure PE and CL systems was investigated in detail [9,10,11,12,13]. Both these lipids are characterized by a cross-sectional area of the headgroup region smaller than the one associated to the acyl chain region, therefore exhibiting an overall conical shape (Figure 1). The molecular shape associated with the PE and CL lipids is responsible for their tendency to form inverse hexagonal phases under certain pH and ionic strength conditions. In the bacterial cytoplasmic membrane, PE and CL lipids favor the formation of high-curvature regions and CL, in particular, is accumulated at the poles of the cylindrical bacterial cells [14,15]. The binary mixtures PE/CL, [12,16,17,18] PC/CL, [18,19,20] PE/PG, [20,21,22] and PG/CL [23] have also been previously characterized by means of several techniques, such as differential scanning calorimetry, X-ray scattering, fluorescence spectroscopy, surface-sensitive techniques, Langmuir isotherms, atomic force microscopy, infrared spectroscopy, as well as molecular dynamics simulations. In the above- studies, PE, PC, PG and CL lipids with different composition of the acyl chains were used: PE, PC and PG exhibited acyl chains with 14-18 C atoms and 0-1 unsaturations, i.e. oleyl, palmitoyl, myristoyl fatty acids, while CL lipids were either tetramyristoyl-cardiolipin (TMCL) or bovine heart CL. Although the acyl chain composition is responsible for specific physical properties of the lipid bilayer, a general description of the effect of cardiolipin on phospholipid bilayers can still be extrapolated. Addition of 5-20 mol % of CL to PC, PE and PG lipids results in the formation of stable lamellar phases. In the binary mixtures of

CL with PE, PC or PG lipids, the favorable hydrogen bonds between the CL headgroup and the surrounding phospholipid headgroups retrieve the PE, PC and PG lipids around the CL molecules[13]. As a consequence, the bilayer thickness is increased compared to pure PE, PC, PG bilayers. A similar condensing effect was previously reported in the case of cholesterol-containing lipid bilayers [24]. In addition, in case of PC-lipids with short and saturated acyl chains, i.e. 1,2-dimyristoyl-sn-glycero-3-phosphorylcholine (DMPC), both cholesterol and CL increase the bilayer order parameter thus reducing the membrane fluidity above the DMPC melting temperature (T_m=25ºC)[25]. However, in case of PC-lipids with longer and unsaturated acyl chains, i.e. POPC or egg-PC, while cholesterol still increases the acyl chain order parameter[26,27], CL shows an opposite effect [28]. To the best of our knowledge, only a few studies have been reported in which ternary mixtures of PE, PG and CL lipids were used. These latter focused on the thermotropic behavior of PE/PG/CL mixtures[29], the structure of lipid monolayer at air/water interface[30] or directly implemented PE/PG/CL mixtures to investigate the activity of an antimicrobial agent[31, 32, 33]. Therefore, a detailed structural and dynamic characterization of PE/PG/CL mixtures is still missing.

In the present study, we show the preparation and characterization of vesicles containing mixtures of POPE/POPG/CL with composition 60/30/10 mol/mol/mol and 50/30/20 mol/mol/mol, named hereafter POPE/POPG/CL10 and POPE/POPG/CL20. The binary mixture POPE/POPG (70/30 mol/mol) was also characterized and used as a reference sample. As the cytoplasmic membrane from most bacteria, the investigated vesicles exhibit PE as the main component, followed by PG and with CL as minor component. More specifically, the used lipid ratios make the POPE/POPG/CL10 and POPE/POPG/CL20 vesicles relevant model of the cytoplasmic membrane from common Gram-negative bacteria, such as *Escherichia Coli*[34] and *Pseudomonas*

aeruginosa[35]. Small angle neutron scattering (SANS) and dynamic light scattering (DLS) measurements were combined to investigate the size and polydispersity of the prepared vesicles as well as to extract information on the structure of the lipid bilayers as a function of the CL content. In addition, electron paramagnetic resonance (EPR) spectroscopy was used to investigate the dynamics of the different lipid mixtures. In the EPR experiments, spin-labelled lipids were added to the above-listed phospholipid mixtures. Different types of spin-labelled lipids were chosen with the radical nitroxide group bound to different positions along the lipid acyl chain (Supporting Information (SI), Figure S1). Therefore, the collected EPR spectra provided a detailed description of the lipid packing and fluidity across the bilayers. SANS, DLS and EPR measurements were all performed at 25 °C with the lipid vesicles in the physiological buffer with composition 150 mM sodium chloride, 10 mM HEPES, 1mM calcium chloride and pH=7.2.

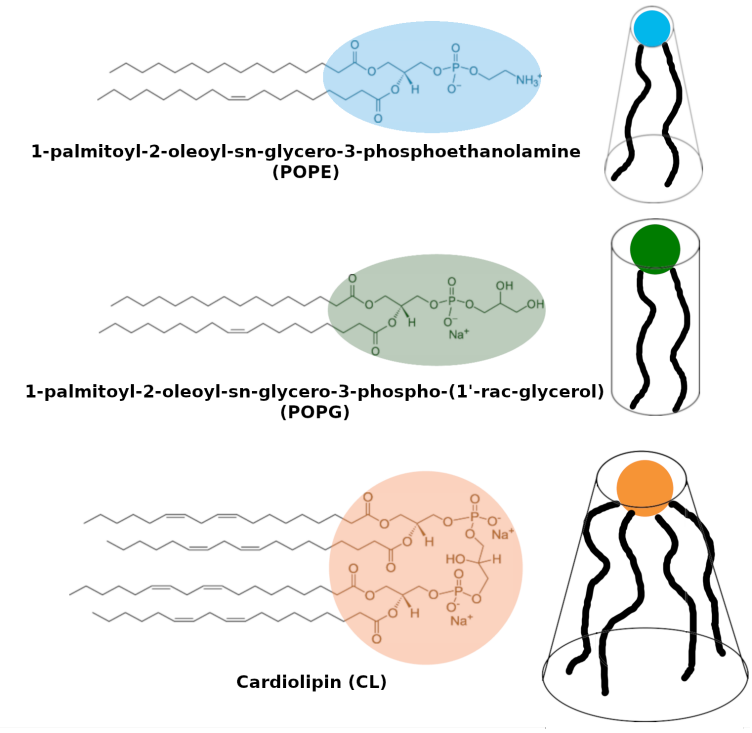

Figure 1 - Molecular structures, together with the cartoon representation including the molecule geometrical shape, of POPE, POPG and CL phospholipids.

Altogether, we show that CL induces the formation of thicker lipid bilayers compared to the binary POPE/POPG mixture and also increases membrane curvature. We also report that CL reduces the order parameter associated to the lipid bilayer compared to the binary POPE/POPG mixture, thus increasing the membrane fluidity. All these effects are dependent on the CL concentration in the lipid bilayer.

Materials and Methods

Materials

Dichloromethane and methanol, HPLC-grade solvents, were obtained from Merck (Darmstadt, Germany) while D_2O (isotopic enrichment > 99.8%, molar mass 20.03 g mol^{-1}) was purchased from Sigma (Milan, Italy). 1-palmitoyl-2-oleoyl-*sn*-glycero-3-phosphoethanolamine (POPE, 99 % purity) and 1-palmitoyl-2-oleoyl-*sn*-glycero-3-phosphoglycerol (POPG, 99% purity) were obtained from Avanti Polar Lipids (Alabaster, USA), while cardiolipin (CL, ≥97 % purity) were obtained from Sigma-Aldrich (Milan, Italy). HEPES buffer solution (10 mM), NaCl and $CaCl_2$ salt were obtained from Sigma-Aldrich (Milan, Italy). Spin-labelled phosphatidylcholines (*n*-PCSL) with the nitroxide group at different positions (*n*= 5, 7, 10 and 14) in the *sn*-2 acyl chain (Figure SI1), to be used for EPR experiments, were also purchased from Avanti Polar Lipids (Alabaster, USA) and stored at -20 °C in ethanol solutions at a concentration of 1 mg/mL.

Sample Preparation

Small Unilamellar Vesicles (SUVs) composed by POPE, POPG and CL were prepared with composition 60/30/10 mol% and 50/30/20 mol% (named POPE/POPG/CL10 and

POPE/POPG/CL20). SUV were also prepared with POPE and POPG 70/30 mol/mol. The three phospholipids were independently dissolved in dichloromethane/methanol mixture (2:1 v/v, 10 mg/mL lipid concentration). Proper volumes of these solutions were used to form lipid films with the above reported lipid molar ratios and total lipid amount of 1mg. The lipid films were produced by evaporating the organic solvents under nitrogen flow. Final traces of the solvents were removed by storing the sample under vacuum for at least 3 h. The lipid films were re-suspended with 1mL of physiological buffer (with composition sodium chloride, 150 mM, HEPES 10 mM, 1mM calcium chloride, 1mM, and pH=7.2), and repeatedly vortexed. The produced Multi Lamellar Vesicles (MLVs) were repeatedly extruded through polycarbonate membranes of 100 nm pore size, for at least 11 times, before DLS, SANS measurements in order to produce SUV suspensions. A buffer with the above-reported composition but prepared with D_2O was used in the case of samples for SANS measurements.

The same protocol was used to prepare SUV samples for EPR measurements, but a proper volume of each stock solution in ethanol (1 mg/mL) of spin-labelled phosphatidylcholines (n-PCSL) was also added to the lipid films in order to have a spin-label content equal to 1 wt. % of the total lipids. The prepared 1 mg lipid films containing n-PCSLs were dissolved with 50 μL of buffer (150 mM, HEPES 10 mM, 1mM calcium chloride, 1mM, and pH=7.2) and treated as described above to produce SUV suspensions.

Small Angle Neutron Scattering (SANS)

SANS measurements were performed at 25 °C at the KWS2 instrument located at the Heinz Maier-Leibnitz Source, Garching Forschungszentrum (Germany) [36]. Neutrons with a wavelength spread ($\Delta\lambda/\lambda$) 0.1 were used. A two-dimensional array detector at three different wavelength

(W)/collimation (C) /sample-to-detector(D) distance combinations ($W_{7Å}C_{8m}D_{2m}$, $W_{7Å}C_{8m}D_{8m}$ and $W_{19Å}C_{8m}D_{8m}$), measured neutrons scattered from the samples. These configurations allowed us to collect data in a range of the scattering vector modulus $q = \frac{4\pi sin(\theta/2)}{\lambda}$, 0.002-0.4 Å^{-1}, with scattering angle θ. The investigated systems were contained in a closed quartz cell, and, for each sample, data were collected for a sufficient time such to have ~ 2 million counts over the entire detection area. The raw data were corrected for detector sensitivity, blocked-beam, background and empty cell scattering, followed by the radial averaging and transformation to absolute scattered intensity ($I(q)$) using a secondary plexiglass standard[30,31].

Generally, the dependence of the absolute scattered intensity from the scattering vector is:

$$I(q) = \frac{\phi_p}{V_p} P(q)S(q) + Bkg \quad (1)$$

where ϕ_p and V_p are the particle volume fraction and the particle volume, while $P(q)$ and $S(q)$ are the form factor and the structure factor, respectively. The last term (Bkg) takes into account the incoherent scattering mostly due to the presence of hydrogen atoms within the sample.

The form factor describes the shape and size distribution of the scattering particles. On the other hand, the structure factor accounts for interparticle correlations within the sample. The structural information contained in both the form and the structure factor can be expressed by choosing an appropriate model to fit the experimental data.In the present case, the vesicle suspensions were sufficiently diluted to consider interparticle correlations negligible and thus $S(q)$=1. SANS data were analyzed with an in-house developed code. Further details about data analysis are reported in supporting information.

Dynamic Light Scattering (DLS)

DLS measurements were performed with a home-made instrument composed of a Photocor compact goniometer, a SMD 6000 Laser Quantum 50 mW light source operating at 5325 Å, a photomultiplier (PMT-120-OP/B) and a correlator (Flex02-01D) from Correlator.com. The experiments were carried out at the constant temperature (25.0 ± 0.1) °C, by using a thermostatic bath, and at the scattering angle θ of 90°. The correlation function of the scattered intensity was analyzed using a regularization algorithm [37]. The diffusion coefficient (*D*) of each population of diffusing particles was calculated as the z-average of the diffusion coefficients of the corresponding distributions [38,39]. Considering that the solutions are dilute, the particle hydrodynamic radius, R_H, can be estimated from the Stokes–Einstein equation

$$R_H = \frac{k_B T}{6\pi\eta D} \quad (2)$$

where k_B is the Boltzmann constant, T is the temperature and η is the solvent viscosity. For non-spherical particles, R_H corresponds to the radius of a spherical particle with the same diffusion coefficient measured.

Electron Paramagnetic Resonance (EPR) spectroscopy

EPR spectra were recorded with a 9 GHz Bruker Elexys E-500 spectrometer (Bruker, Rheinstetten, Germany). The capillaries containing the vesicle suspensions were placed in a standard 4 mm quartz sample tube containing light silicone oil for thermal stability. All the measurements were performed at 25 °C. Spectra were recorded using the following instrumental settings: sweep width, 100 G; resolution, 1024 points; time constant, 20.48 ms; modulation frequency, 100 kHz; modulation amplitude, 1.0 G; incident power, 6.37 mW. Several scans, typically 16, were accumulated to improve the signal-to-noise ratio. A quantitative analysis of n-PCSL spectra for all the lipid mixtures was realized determining the acyl chain order parameters relative to the bilayer

normal, S, and the isotropic hyperfine coupling constants for the spin-labels in the membrane, a'_N, following a previously described analytic approach [40,41].

Results and discussion

Small angle neutron scattering and dynamic light scattering characterization

Figure 2a and b show the collected experimental data for the POPE/POPG and the POPE/POPG/CL suspensions containing either 10 or 20 mol % of CL, i.e., POPE/POPG/CL10 and POPE/POPG/CL20. For all the investigated samples, the same theoretical model was used to interpret the collected data. A first inspection of the data in the high-q region, 0.02-0.4 $Å^{-1}$, suggested the presence in the samples of small unilamellar vesicles. On the other hand, the observed linear increase of the scattered intensity in the low-q region, 0.003-0.01 $Å^{-1}$, indicated the presence of larger particles in the suspension, although their averaged size and shape cannot be deduced from the data in the explored q range. These larger particles were interpreted as vesicle aggregates. Indeed, no model referring to multilamellar objects resulted suitable to fit the experimental SANS profiles. In addition, it was previously reported that, in the presence of salts, unilamellar lipid vesicles can assemble into larger aggregates with fractal structure. [42] Therefore, the model used to analyze the collected data contains the sum of two contributions: the unilamellar vesicle form factor [43], in order to describe the high-q region, and a power law, in order to describe the contribution to the scattered intensity from the larger particles (equations 3 and 4).

$$I(q) = \frac{\phi_{shell}}{V_{shell}} P_{vesicle}(q) + Aq^{-m} \tag{3}$$

$$P_{vesicle}(q) = \left[3V_{core}(\rho_{buffer} - \rho_{shell}) \frac{\sin(qr_{core}) - qr_{core}\cos(qr_{core})}{(qr_{core})^3} + 3V_{shell}(\rho_{shell-}\rho_{buffer}) \frac{\sin(qr_{shell}) - qr_{shell}\cos(qr_{shell})}{(qr_{shell})^3} \right]^2 \tag{4}$$

In equation 3 and 4, ϕ_{shell} and V_{shell} are the volume fraction and the total volume of the lipids composing the shell of the unilamellar vesicles, respectively. ρ_{buffer} and ρ_{shell} are the scattering length densities of the buffer, which is the dispersing medium and is also present in the core of the vesicles, and of the lipids in the vesicle shell. The scattering length densities of the buffer and the lipids was calculated according to their composition as $5.9 \cdot 10^{-6}$ Å^{-2} and $3.2 \cdot 10^{-6}$ Å^{-2} respectively. Because of the similar chemical composition of the POPE, POPG and CL molecules, the same value for ρ_{shell} was obtained for the POPE/POPG, POPE/POPG/CL10 and POPE/POPG/CL20 mixtures. Finally, V_{core} is the volume of the vesicle core, and r_{core} and r_{shell} are the radius of the vesicle core and the thickness of the vesicle lipid shell, i.e., lipid bilayer thickness. In the power law term of equation 2, A is a pre-exponential factor, and m is the exponent of the power law. To properly describe the experimental data, the polydispersity associated to the vesicle size distribution and the instrument resolution was included in the model (see SI).

Optimization of the model parameters produced a good agreement between the fitting curves and the experimental data. In all cases, the power law exponent resulted to be ~ -3, consistent with fractal aggregates composed of vesicles (Figure 2). Fitting the model to the experimental data also confirmed the presence of unilamellar vesicles in the investigated suspensions with the structural parameters reported in Table 1.

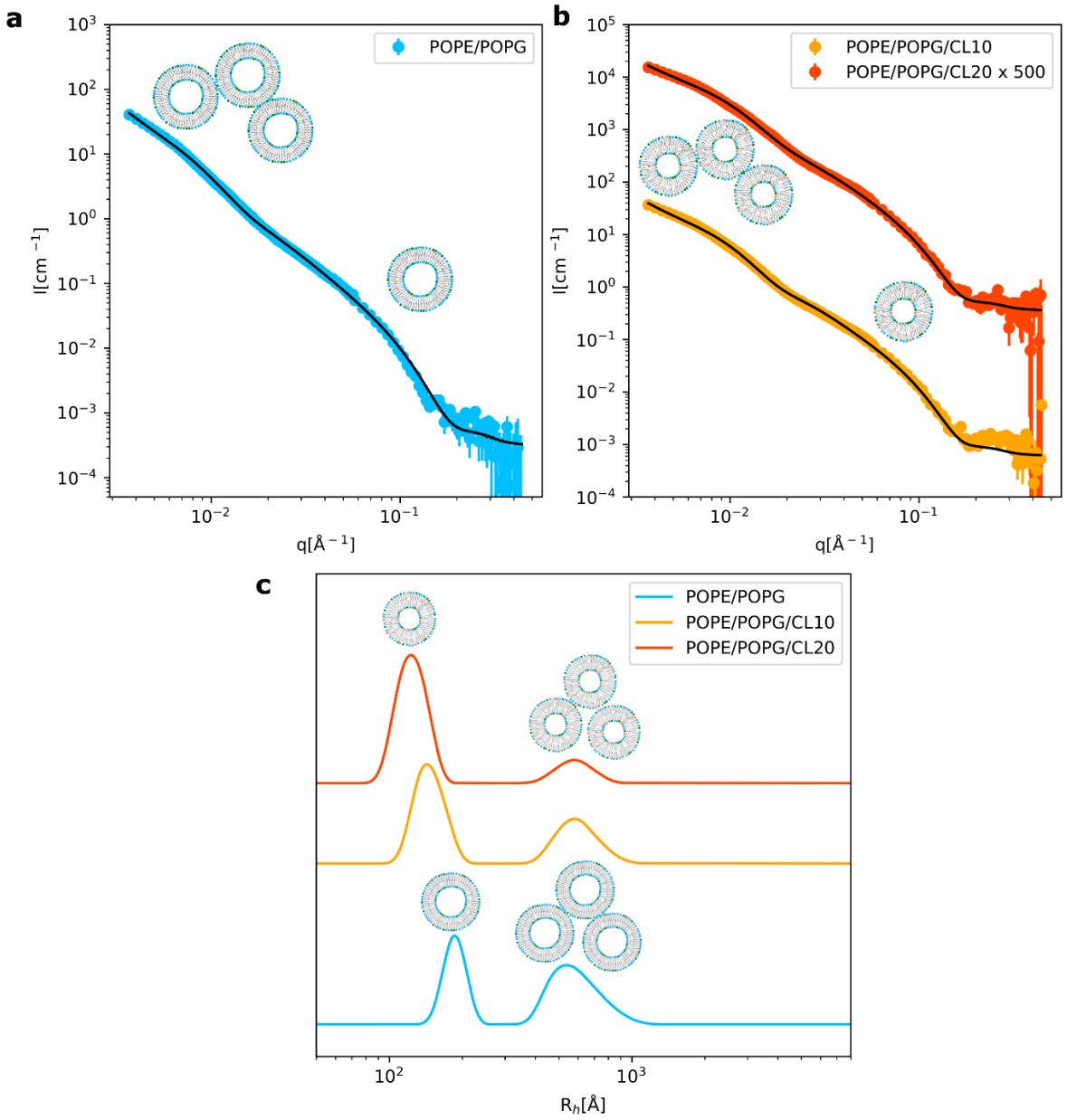

Figure 2 - SANS experimental data together with the corresponding fitting curve for the POPE/POPG (70/30 mol/mol) vesicle suspension (**a**) and the POPE/POPG/CL (60/30/10 mol/mol/mol) and POPE/POPG/CL (50/30/20 mol/mol/mol) vesicle suspension (**b**). Data in (**b**) were scaled for visualization. A cartoon representation of the sample structures corresponding to the low and high q-range, i.e., vesicle aggregates and isolated vesicles, is reported both in (**a**) and (**b**). Hydrodynamic radius distribution extracted from the DLS measurements on the vesicle suspension are reported in (**c**).

Table 1 - Structural parameters (i.e. core radius, core radius polydispersity and bilayer thickness) of the unilamellar vesicles estimated from the analysis of the SANS data collected for the investigated samples. Hydrodynamic radius of the vesicle aggregates estimated from the DLS measurements.

Parameters	**POPE/POPG**	**POPE/POPG/CL10**	**POPE/POPG/CL20**
Vesicle core radius (Å)	149 ± 2	130 ± 1	108 ± 2
Core radius Polydispersity	0.40 ± 0.01	0.35 ± 0.02	0.44 ± 0.09
Bilayer thickness (Å)	34 ± 1	37 ± 1	38 ± 1
Vesicle hydrodynamic radius (Å)	200 ± 30	140 ± 20	110 ± 20
Vesicle aggregate hydrodynamic radius (Å)	570 ± 20	550 ± 20	510 ± 60

Inspection of Table 1 indicates that both the vesicle size and the bilayer thickness are sensitive to the presence of CL in the mixture with POPE and POPG. Indeed, a systematic decrease of the vesicle core radius and parallel increase of the bilayer thickness resulted dependent on the CL concentration. In particular, at CL concentration 20 % mol very small vesicles are formed with core radius ~ 108 Å, compared to the larger vesicles observed in the case of the POPE/POPG suspension, i.e. core radius corresponding to ~ 149 Å. The observed decrease of the vesicle core radius is consistent with the tendency of CL to accumulate in high-curvature regions of biological membranes [44]. The observed increment of the bilayer curvature in the vesicles also suggests that, at high concentrations, CL is most likely present in the inner bilayer leaflet compared to the outer bilayer leaflet, although the available experimental data does not allow to directly quantify the CL

content in the two bilayer leaflets. Indeed, the inner leaflet will allow the lipid bilayer to bend and form vesicles with a smaller core radius compared to the POPE/POPG mixture. CL not only affects the vesicle size, but also impacts the lipid bilayer structure. Indeed, the presence of CL in mixture with POPE and POPG produced thicker lipid bilayers (~ 37 Å) compared to the POPE/POPG mixture (~ 34 Å). The increment of the bilayer thickness can be associated with the dense packing of the surrounding phospholipid molecules, which favors the formation of hydrogen bonds with the CL headgroup.

DLS measurements were performed to complement the SANS characterization and provide a more detailed structural description of the large vesicle aggregates in terms of their hydrodynamic radius (R_h). The scattered intensity measured in the DLS experiment depends on both the mass (M) squared and the concentration of the scattering objects. In the present case, we are dealing with spherical objects, so that $M \approx k\, R_h^3$. Figure 2c shows the hydrodynamic radius distribution obtained by normalizing the scattering intensity for the squared mass of the scattering particle[37].

DLS confirmed the presence of two particle populations in all the investigated vesicle suspensions. The two particle populations have considerably different averaged diffusion coefficients and therefore corresponding hydrodynamic radii (Table 1). The most abundant population is characterized by an estimated hydrodynamic radius comparable with the vesicle radius obtained from the SANS data analysis. This population corresponds to the unilamellar vesicles, which was probably the most favorable organization of lipids and showed a decreasing hydrodynamic radius with increasing CL concentration in the lipid mixture. In all the investigated samples, the second particle population, corresponding to the vesicle aggregates, showed a larger averaged hydrodynamic radius (~ 500-580 Å). The vesicle aggregate population exhibited similar hydrodynamic radius values for all the investigated samples (Table 1).

Electron Paramagnetic Resonance analysis

Figure 3a and b shows the EPR spectra collected to analyze the impact of CL (at 10 and 20 % mol) on the packing and dynamics of POPE/POPG bilayers. The vesicle suspensions used for the EPR measurements were prepared by alternatively incorporating in lipid mixtures 1 mol % of phosphatidylcholines spin-labelled at the different positions of the s*n*-2 chain (n-PCSL, with n = 5, 7, 10 or 14). Specifically, 5-PCSL exhibits a nitroxide group close to the hydrophilic lipid headgroups, 7-PCSL and 10-PCSL are representative of the intermediate segments of the lipid acyl chains, while in 14-PCSL the nitroxide group is positioned close to the terminal methyl groups. Therefore, the combined use of different *n*-PCSL spin-labels enabled us to characterize both the outer and inner bilayer regions. The analysis of the collected spectra provided information about the local microstructure and polarity of the investigated lipid membranes.

For all the characterized lipid mixtures, the spectra corresponding to the 5-PCSL (Figure 3a) show a clearly well-defined axially anisotropic behavior, as detectable by the splitting of the low- and high-field lines. This indicates an ordered organization of the outer segments of the lipid acyl chains. As the reporter nitroxyl group is stepped down along the acyl chain (from position 5 to 10), the spectra anisotropy markedly decreases (Figure 3b) and, in the case of 14-PCSL, a three-line quasi-isotropic spectrum is obtained. This trend was preserved both in the absence and presence of CL within the POPE/POPG mixture. By comparing the n-PCSL spectra of all lipid vesicles, it is possible to note that, when cardiolipin was added to POPE/POPG bilayers, no change was induced in 5- and 7-PCSL spectra which appears very similar. On the other hand, some changes can be appreciated in the line-shapes of 10- and 14-PCSL spectra, which show a reduced anisotropic character. In particular, this effect is much more evident in 14-PCSL spectra of cardiolipin-containing vesicles. Indeed, at both CL contents, the EPR signals show a pronounced

isotropic character in which the peaks appear narrower than those of the 14-PCSL spectrum corresponding to pure POPE/POPG bilayer. This evidence indicates a faster motion of the spin-labelled segment of the lipid chains.

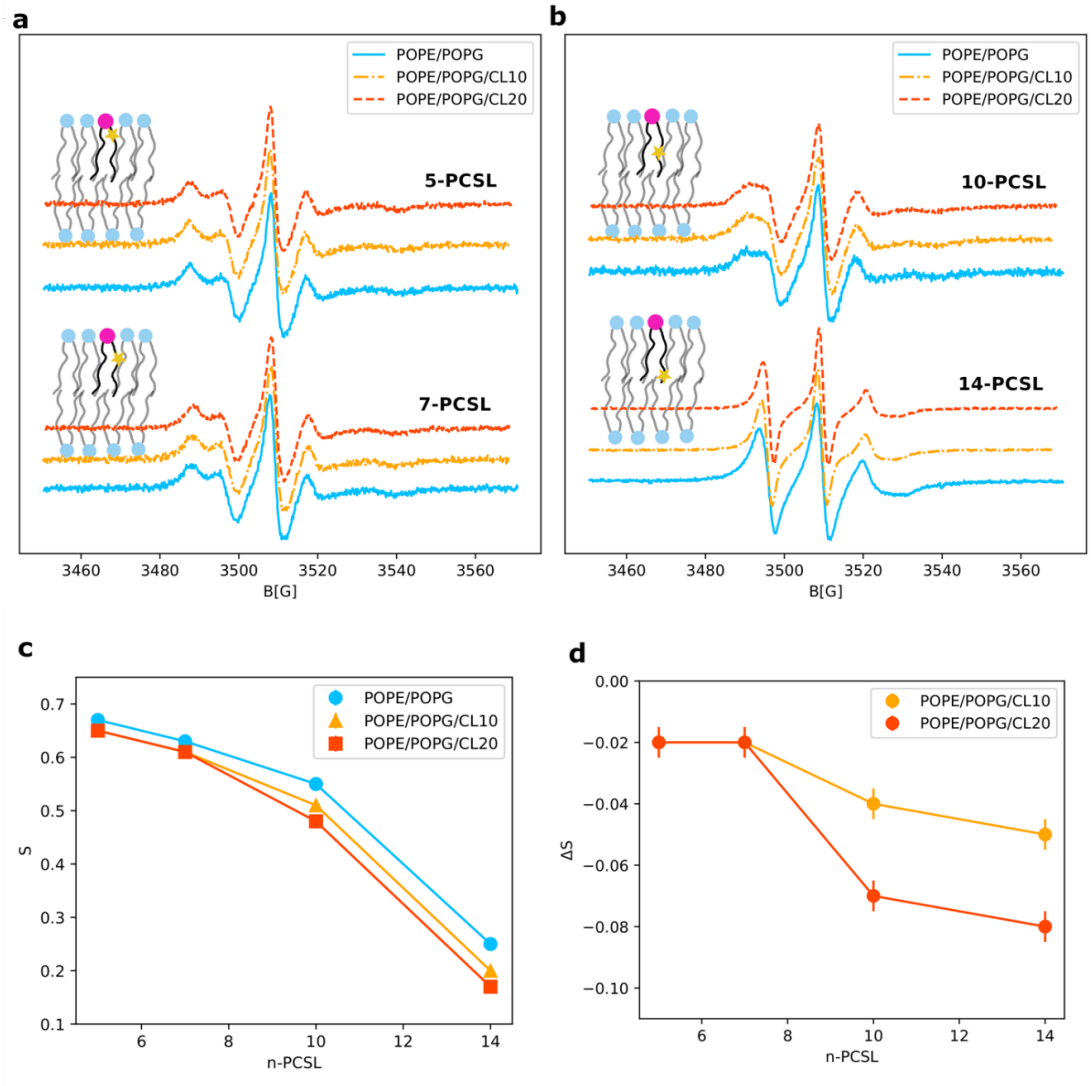

Figure 3 - (**a**) and (**b**) EPR spectra of n-PCSL in POPE/POPG mixture without (continuous lines) and with CL at 10 % mol (pointed lines) and 20 % mol (dotted lines). In the cartoon representation of the investigated samples, the n-PCSL is represented with a magenta-colored headgroup and star is used to indicate the position of the nitroxyl group along the acyl chain. (**c**) Profiles of the order parameter, *S*, as function of n-position for the POPE/POPG mixture without and with CL at 10 %

mol and 20 % mol. (**d**) Variation of *S*, with respect to the POPE/POPG bilayer, on adding CL at different content.

In order to quantitatively analyze the spectra, the order parameter, *S*, and the isotropic hyperfine coupling constant, a_N, were evaluated (Table 2) as previously described in the literature.[40,41,45] *S* is a measure of the local orientational ordering of the labelled acyl chain with respect to the normal to the bilayer surface, while a_N is an index of the micro-polarity experienced by the nitroxide. Both these parameters allowed us to monitor changes in the microstructure of the phospholipid bilayers as function of the CL concentration. In particular, Figure 3c shows the dependence of *S* on the chain position, *n*, of the nitroxyl group in the *n*-PCSL spin-labels. A decrease in the *S* values of *n*-PCSL spectra for POPE/POPG/CL bilayers was observed for both the considered CL concentrations, indicating a decrease in the packing ordering of phospholipids involving the whole bilayer. However, this effect is more much evident for 10- and 14-PCSL and by increasing the CL content. These differences can be appreciated by observing the trends of the *S* variation (ΔS), determined with respect to the value determined in the absence of CL, as shown in Figure 3d. For both lipid samples, the order parameter *S* decreases with the same extent (ΔS of ~ -0.02) for both 5- and 7-PCSL spectra. In the case of POPE/POPG/CL10 bilayers, the order parameter decreases with a greater extent for both 10- and 14-PCSL spectra, as demonstrated by ΔS values of ~0.04 and ~ -0.05, respectively. This suggested that the CL content of 10 mol% induce a more disordered lipid-packing in the inner region of POPE/POPG bilayer, probably due to a reorganization of acyl chains. On the other hand, the presence of CL at 20 mol% in POPE/POPG bilayer causes a stronger effect on the order parameter for 10- and 14-PCSL, as indicated by ΔS values of about -0.07 and -0.08, respectively, confirming the fluidifying role of high CL content on the whole bilayer. To analyze the 14-PCSL spectrum, variations in deeper details, a computational analysis (reported in

Figure S2) was realized by using a well-established procedure described by Budil et al.[46] As indicated by the values of the main parameters used for the simulations (see Table S1), such as the order parameter (*S*) and the correlation time for the rotational diffusion motion (τ_{perp}), both the lipid-bilayer order and micro-viscosity decreased in the presence of CL in a concentration dependent manner, thus confirming a greater fluidity of POPE/POPG/CL20 bilayers with respect to pure POPE/POPG ones.

Table 2 - Values of order parameter, *S*, and hyperfine coupling constant, a'_N, for EPR spectra of n-PCSL in POPE/POPG bilayers without and with CL at different lipid composition.

n-PCSL	**POPE/POPG**	**POPE/POPG/CL10%**	**POPE/POPG/CL20%**
		S	
5-PCSL	0.67 ± 0.01	0.65 ± 0.01	0.65 ± 0.01
7-PCSL	0.63 ± 0.01	0.61 ± 0.01	0.61 ± 0.01
10-PCSL	0.55 ± 0.01	0.51 ± 0.01	0.48 ± 0.01
14-PCSL	0.25 ± 0.01	0.20 ± 0.01	0.17 ± 0.01
		a'_N **(G)**	
5-PCSL	15.4 ± 0.1	15.2 ± 0.1	15.1 ± 0.1
7-PCSL	15.3 ± 0.1	15.0 ± 0.1	14.9 ± 0.1
10-PCSL	15.1 ± 0.1	14.6 ± 0.1	14.5 ± 0.1
14-PCSL	14.2 ± 0.2	13.8 ± 0.2	13.9 ± 0.2

Finally, as observed in Table 2, a'_N values decrease with n-PCSL, indicating that the hydrophobicity increases as the nitroxide group moves to the center of the bilayer; the CL presence in POPE/POPG

bilayers induces a reduction in the micro-polarity which could be associated to a lower penetration of water molecules as a consequence of a slightly different lipid packing in the mixtures containing CL. This trend was also confirmed by the values of average hyperfine coupling constant, <A>, obtained from the simulations of 14-PCSL spectra (see Table S2). Only slight differences are observed in the spectra if bivalent cations, i.e. Ca^{2+}, are removed from the buffer (Figure SI3), the general trends being the same discussed above.

Conclusion

The bacterial cytoplasmic membrane, and in particular the anionic phospholipids, i.e. PG and CL, are often used as targets for antimicrobial agents, which induce membrane lysis and therefore the death of the bacteria[8]. However, because of the growing resistance towards antibacterial drugs, understanding the structural and dynamic properties of the bacterial cytoplasmic membrane can provide important inputs for the design of new and more efficient antimicrobial agents.

The physico-chemical characterization of lipid systems mimicking the bacterial cytoplasmic membrane has been so far focused on simple lipid mixtures including only 1-2 lipid species, e.g. PE/PG and PE/CL mixtures[13]. To the best of our knowledge, very few studies have been reported on tertiary PE/PG/CL mixtures, which represent a better mimic of the bacterial cytoplasmic membrane compared to the above-mentioned binary mixtures[29,30,31]. This prompted us to investigate POPE/POPG/CL vesicle suspensions with different CL concentration, i.e. 10 and 20 % mol, and to perform a detailed structural and dynamic characterization of the prepared samples by means of SANS, DLS and EPR experiments.

According to the collected SANS and DLS data, all the characterized vesicle suspensions resulted to be composed by unilamellar vesicles together with larger vesicle aggregates, i.e. 500-

580 Å hydrodynamic radii. The presence of CL in the POPE/POPG mixture produced a systematic decrease of the vesicle core radius and therefore increment of the membrane curvature (Table 1). This evidence is consistent with the previously reported sorting of CL in high-curvature regions in bacterial membranes. CL is also responsible for the increment of the bilayer thickness, in the presented cases of ~3 Å (Table 1).

On the other hand, EPR spectroscopy was used to investigate the impact of CL on the membrane fluidity and lipid packing. The addition of CL in the POPE/POPG mixtures decreases the order parameter of the membrane compared to POPE/POPG. In addition, the use of different spin-labelled phosphatidylcholines (n-PCSL), exhibiting the nitroxyl group covalently bonded to the lipid acyl chain at different positions, allowed us to appreciate significant differences in the lipid packing when the CL content is 10 or 20 % mol. Indeed, at 10 % mol CL mainly perturbs the packing and fluidity of the acyl chain in the inner region of the bilayer while the effect propagates to the entire acyl chain region when the CL concentration is increased to 20 % mol.

Increasing the amount of CL in the cytoplasmic membrane is a known strategy of bacteria to enhance the membrane structural integrity and therefore the bacteria resistance towards antimicrobial agents such as daptomycin and surfactin.[47, 48] In our model systems composed by POPE/POPG/CL, we found that increasing CL concentrations affect the phospholipid packing and produce thicker and more fluid bilayers, which can accommodate higher membrane curvature. Therefore, our results support the proposed role of CL in preventing the membrane penetration by drugs and enhancing the membrane stability towards the increased curvature often produced by the drug-membrane interaction. In this respect, the discussed data suggests that future antimicrobial drug development should focus on overcoming this stabilizing effect of CL to produce molecules with more efficient penetration properties also in the case of highly curved

membranes. From this point of view, the characterized bacterial membrane models can be used as relevant lipid-platforms for testing antimicrobial drug activity.

ASSOCIATED CONTENT

Supporting Information. Further details on SANS data analysis and additional EPR data.

AUTHOR INFORMATION

Corresponding Authors

*Giuseppe Vitiello

Department of Chemical, Materials and Production Engineering, University of Naples Federico II, Piazzale Tecchio 80, 80125 Naples, Italy.

giuseppe.vitiello@unina.it

*Alessandra Luchini

Paul Scherrer Insitut Forschungsstrasse 111, 5232 Villigen, Switzerland

alessandra.luchini@psi.ch

Present Addresses

†Paul Scherrer Insitut, Forschungsstrasse 111, 5232 Villigen, Switzerland

Author Contributions

The manuscript was written through contributions of all authors. All authors have given approval to the final version of the manuscript

ACKNOWLEDGMENT

This work is based upon experiments performed at the KWS-2 instrument operated by JCNS at the Heinz Maier-Leibnitz Zentrum (MLZ), Garching, Germany. The authors thank the MLZ for provision of beam time**.** The authors also thank Prof. Maria Francesca Ottaviani (University of Urbino) for the help in simulating the EPR spectra.

REFERENCES

1. Epand, R. M.; Epand, R. F. Bacterial membrane lipids in the action of antimicrobial agents. *Journal of Peptide Science* **2011,** *17* (5), 298-305.
2. Luchini, A.; Vitiello, G. Mimicking the Mammalian Plasma Membrane: An Overview of Lipid Membrane Models for Biophysical Studies. *Biomimetics* **2021,** *6* (1), 3.
3. Strahl, H.; Errington, J. Bacterial Membranes: Structure, Domains, and Function. *Annu Rev Microbiol* **2017,** *71*, 519-538.
4. Mykytczuk, N. C. S.; Trevors, J. T.; Leduc, L. G.; Ferroni, G. D. Fluorescence polarization in studies of bacterial cytoplasmic membrane fluidity under environmental stress. *Progress in Biophysics and Molecular Biology* **2007,** *95* (1), 60-82.
5. Grogan, D. W.; Cronan, J. E. Cyclopropane ring formation in membrane lipids of bacteria. *Microbiology and Molecular Biology Reviews* **1997,** *61* (4), 429-441.
6. Schlame, M. Thematic review series: Glycerolipids - Cardiolipin synthesis for the assembly of bacterial and mitochondrial membranes. *J Lipid Res* **2008,** *49* (8), 1607-1620.
7. Romantsov, T.; Wood, J. M. Contributions of Membrane Lipids to Bacterial Cell Homeostasis upon Osmotic Challenge. In *Biogenesis of Fatty Acids, Lipids and Membranes*, Geiger, O., Ed.; Springer International Publishing: Cham, 2016, pp 1-22.
8. Nordström, R.; Malmsten, M. Delivery systems for antimicrobial peptides. *Advances in colloid and interface science* **2017,** *242*, 17-34.
9. Picas, L.; Montero, M. T.; Morros, A.; Oncins, G.; Hernandez-Borrell, J. Phase changes in supported planar bilayers of 1-palmitoyl-2-oleoyl-sn-glycero3-phosphoethanolamine. *J Phys Chem B* **2008,** *112* (33), 10181-10187.
10. Shalaev, E. Y.; Steponkus, P. L. Phase diagram of 1,2-dioleoylphosphatidylethanolamine (DOPE):water system at subzero temperatures and at low water contents. *Biochimica et Biophysica Acta (BBA) - Biomembranes* **1999,** *1419* (2), 229-247.
11. Thurmond, R. L.; Lindblom, G.; Brown, M. F. Curvature, order, and dynamics of lipid hexagonal phases studied by deuterium NMR spectroscopy. *Biochemistry* **1993,** *32* (20), 5394-410.
12. Dahlberg, M. Polymorphic phase behavior of cardiolipin derivatives studied by coarse-grained molecular dynamics. *J Phys Chem B* **2007,** *111* (25), 7194-7200.
13. Lewis, R. N.; McElhaney, R. N. The physicochemical properties of cardiolipin bilayers and cardiolipin-containing lipid membranes. *Biochimica et biophysica acta* **2009,** *1788* (10), 2069-79.
14. El Khoury, M.; Swain, J.; Sautrey, G.; Zimmermann, L.; Van Der Smissen, P.; Décout, J.-L.; Mingeot-Leclercq, M.-P. Targeting Bacterial Cardiolipin Enriched Microdomains: An Antimicrobial Strategy Used by Amphiphilic Aminoglycoside Antibiotics. *Scientific Reports* **2017,** *7* (1), 10697.
15. Oliver, P. M.; Crooks, J. A.; Leidl, M.; Yoon, E. J.; Saghatelian, A.; Weibel, D. B. Localization of Anionic Phospholipids in Escherichia coli Cells. *Journal of Bacteriology* **2014,** *196* (19), 3386-3398.
16. Frias, M.; Benesch, M. G. K.; Lewis, R. N. A. H.; McElhaney, R. N. On the miscibility of cardiolipin with 1,2-diacyl phosphoglycerides: Binary mixtures of dimyristoylphosphatidylethanolamine and tetramyristoylcardiolipin. *Biochimica et Biophysica Acta (BBA) - Biomembranes* **2011,** *1808* (3), 774-783.

17. Lupi, S.; Perla, A.; Maselli, P.; Bordi, F.; Sennato, S. Infrared spectra of phosphatidylethanolamine–cardiolipin binary system. *Colloids and Surfaces B: Biointerfaces* **2008,** *64* (1), 56-64.
18. Dahlberg, M.; Maliniak, A. Mechanical Properties of Coarse-Grained Bilayers Formed by Cardiolipin and Zwitterionic Lipids. *J Chem Theory Comput* **2010,** *6* (5), 1638-1649.
19. Domènech, Ò.; Sanz, F.; Montero, M. T.; Hernández-Borrell, J. Thermodynamic and structural study of the main phospholipid components comprising the mitochondrial inner membrane. *Biochimica et Biophysica Acta (BBA) - Biomembranes* **2006,** *1758* (2), 213-221.
20. Schmidt, T. F.; Caseli, L.; Oliveira, O. N.; Itri, R. Binding of Methylene Blue onto Langmuir Monolayers Representing Cell Membranes May Explain Its Efficiency as Photosensitizer in Photodynamic Therapy. *Langmuir* **2015,** *31* (14), 4205-4212.
21. Lind, T. K.; Skoda, M. W. A.; Cárdenas, M. Formation and Characterization of Supported Lipid Bilayers Composed of Phosphatidylethanolamine and Phosphatidylglycerol by Vesicle Fusion, a Simple but Relevant Model for Bacterial Membranes. *ACS Omega* **2019,** *4* (6), 10687-10694.
22. Prossnigg, F.; Hickel, A.; Pabst, G.; Lohner, K. Packing behaviour of two predominant anionic phospholipids of bacterial cytoplasmic membranes. *Biophys Chem* **2010,** *150* (1-3), 129-135.
23. Benesch, M. G. K.; Lewis, R. N. A. H.; McElhaney, R. N. On the miscibility of cardiolipin with 1,2-diacyl phosphoglycerides: Binary mixtures of dimyristoylphosphatidylglycerol and tetramyristoylcardiolipin. *Biochimica et Biophysica Acta (BBA) - Biomembranes* **2015,** *1848* (11, Part A), 2878-2888.
24. Hung, W.-C.; Lee, M.-T.; Chen, F.-Y.; Huang, H. W. The condensing effect of cholesterol in lipid bilayers. *Biophys J* **2007,** *92* (11), 3960-3967.
25. Boscia, A. L.; Treece, B. W.; Mohammadyani, D.; Klein-Seetharaman, J.; Braun, A. R.; Wassenaar, T. A.; Klosgen, B.; Tristram-Nagle, S. X-ray structure, thermodynamics, elastic properties and MD simulations of cardiolipin/dimyristoylphosphatidylcholine mixed membranes. *Chem Phys Lipids* **2014,** *178*, 1-10.
26. Ferreira, T. M.; Coreta-Gomes, F.; Ollila, O. H. S.; Moreno, M. J.; Vaz, W. L. C.; Topgaard, D. Cholesterol and POPC segmental order parameters in lipid membranes: solid state 1H–13C NMR and MD simulation studies. *Physical Chemistry Chemical Physics* **2013,** *15* (6), 1976-1989.
27. Vitiello, G.; Falanga, A.; Petruk, A. A.; Merlino, A.; Fragneto, G.; Paduano, L.; Galdiero, S.; D'Errico, G. Fusion of raft-like lipid bilayers operated by a membranotropic domain of the HSV-type I glycoprotein gH occurs through a cholesterol-dependent mechanism. *Soft matter* **2015,** *11* (15), 3003-16.
28. Unsay, J. D.; Cosentino, K.; Subburaj, Y.; García-Sáez, A. J. Cardiolipin Effects on Membrane Structure and Dynamics. *Langmuir* **2013,** *29* (51), 15878-15887.
29. Lopes, S. C.; Neves, C. S.; Eaton, P.; Gameiro, P. Improved model systems for bacterial membranes from differing species: The importance of varying composition in PE/PG/cardiolipin ternary mixtures. *Molecular Membrane Biology* **2012,** *29* (6), 207-217.
30. Wydro, P. The influence of cardiolipin on phosphatidylglycerol/phosphatidylethanolamine monolayers—Studies on ternary films imitating bacterial membranes. *Colloids and Surfaces B: Biointerfaces* **2013,** *106*, 217-223.

31. Swain, J.; El Khoury, M.; Kempf, J.; Briée, F.; Van Der Smissen, P.; Décout, J.-L.; Mingeot-Leclercq, M.-P. Effect of cardiolipin on the antimicrobial activity of a new amphiphilic aminoglycoside derivative on Pseudomonas aeruginosa. *PLOS ONE* **2018,** *13* (8), e0201752.
32. Juhaniewicz-Dębińska, J.; Dziubak, D.; Sęk, S. Physicochemical Characterization of Daptomycin Interaction with Negatively Charged Lipid Membranes. *Langmuir* **2020,** *36* (19), 5324-5335.
33. Cetuk, H.; Maramba, J.; Britt, M.; Scott, A. J.; Ernst, R. K.; Mihailescu, M.; Cotten, M. L.; Sukharev, S. Differential Interactions of Piscidins with Phospholipids and Lipopolysaccharides at Membrane Interfaces. *Langmuir* **2020,** *36* (18), 5065-5077.
34. Appala, K.; Bimpeh, K.; Freeman, C.; Hines, K. M. Recent applications of mass spectrometry in bacterial lipidomics. *Analytical and Bioanalytical Chemistry* **2020,** *412* (24), 5935-5943.
35. Groenewold, M. K.; Massmig, M.; Hebecker, S.; Danne, L.; Magnowska, Z.; Nimtz, M.; Narberhaus, F.; Jahn, D.; Heinz, D. W.; Jänsch, L.; Moser, J. A phosphatidic acid-binding protein is important for lipid homeostasis and adaptation to anaerobic biofilm conditions in Pseudomonas aeruginosa. *Biochemical Journal* **2018,** *475* (11), 1885-1907.
36. Radulescu, A.; Pipich, V.; Frielinghaus, H.; Appavou, M. S. KWS-2, the high intensity / wideQ-range small-angle neutron diffractometer for soft-matter and biology at FRM II. *Journal of Physics: Conference Series* **2012,** *351*, 012026.
37. Lomakin, A.; Teplow, D. B.; Benedek, G. B. Quasielastic light scattering for protein assembly studies. *Methods in molecular biology (Clifton, N.J.)* **2005,** *299*, 153-74.
38. Zhang, H.; Annunziata, O. Effect of Macromolecular Polydispersity on Diffusion Coefficients Measured by Rayleigh Interferometry. *The Journal of Physical Chemistry B* **2008,** *112* (12), 3633-3643.
39. Luchini, A.; Irace, C.; Santamaria, R.; Montesarchio, D.; Heenan, R. K.; Szekely, N.; Flori, A.; Menichetti, L.; Paduano, L. Phosphocholine-decorated superparamagnetic iron oxide nanoparticles: defining the structure and probing in vivo applications. *Nanoscale* **2016,** *8* (19), 10078-10086.
40. Vitiello, G.; Falanga, A.; Galdiero, M.; Marsh, D.; Galdiero, S.; D'Errico, G. Lipid composition modulates the interaction of peptides deriving from herpes simplex virus type I glycoproteins B and H with biomembranes. *Biochimica et Biophysica Acta (BBA) - Biomembranes* **2011,** *1808* (10), 2517-2526.
41. Vitiello, G.; Zanfardino, A.; Tammaro, O.; Di Napoli, M.; Caso, M. F.; Pezzella, A.; Varcamonti, M.; Silvestri, B.; D'Errico, G.; Costantini, A.; Luciani, G. Bioinspired hybrid eumelanin–TiO2 antimicrobial nanostructures: the key role of organo–inorganic frameworks in tuning eumelanin's biocide action mechanism through membrane interaction. *RSC Advances* **2018,** *8* (50), 28275-28283.
42. Bergström, M.; Pedersen, J. S.; Schurtenberger, P.; Egelhaaf, S. U. Small-Angle Neutron Scattering (SANS) Study of Vesicles and Lamellar Sheets Formed from Mixtures of an Anionic and a Cationic Surfactant. *The Journal of Physical Chemistry B* **1999,** *103* (45), 9888-9897.
43. Guinier, A. a. F., G. *Small angle scattering of X-rays*; John Wiley and Son, New York1955.
44. Beltrán-Heredia, E.; Tsai, F.-C.; Salinas-Almaguer, S.; Cao, F. J.; Bassereau, P.; Monroy, F. Membrane curvature induces cardiolipin sorting. *Communications Biology* **2019,** *2* (1), 225.
45. Merlino, A.; Vitiello, G.; Grimaldi, M.; Sica, F.; Busi, E.; Basosi, R.; D'Ursi, A. M.; Fragneto, G.; Paduano, L.; D'Errico, G. Destabilization of Lipid Membranes by a Peptide Derived

from Glycoprotein gp36 of Feline Immunodeficiency Virus: A Combined Molecular Dynamics/Experimental Study. *The Journal of Physical Chemistry B* **2012,** *116* (1), 401-412.
46. Budil, D. E.; Lee, S.; Saxena, S.; Freed, J. H. Nonlinear-Least-Squares Analysis of Slow-Motion EPR Spectra in One and Two Dimensions Using a Modified Levenberg–Marquardt Algorithm. *Journal of Magnetic Resonance, Series A* **1996,** *120* (2), 155-189.
47. Murínová, S.; Dercová, K. Response mechanisms of bacterial degraders to environmental contaminants on the level of cell walls and cytoplasmic membrane. *Int J Microbiol* **2014,** *2014*, 873081-873081.
48. Zhang, T.; Muraih, J. K.; Tishbi, N.; Herskowitz, J.; Victor, R. L.; Silverman, J.; Uwumarenogie, S.; Taylor, S. D.; Palmer, M.; Mintzer, E. Cardiolipin Prevents Membrane Translocation and Permeabilization by Daptomycin. *Journal of Biological Chemistry* **2014,** *289* (17), 11584-11591.

TOC GRAPHIC

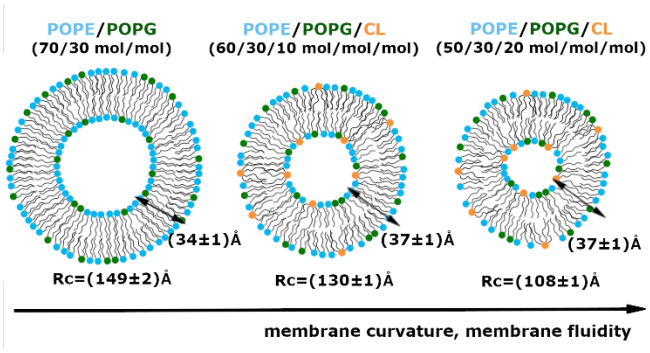
POPE/POPG
(70/30 mol/mol)
POPE/POPG/CL
(60/30/10 mol/mol/mol)
POPE/POPG/CL
(50/30/20 mol/mol/mol)
(34±1)Å
(37±1)Å
(37±1)Å
Rc=(149±2)Å
Rc=(130±1)Å
Rc=(108±1)Å
membrane curvature, membrane fluidity